frontiers in Materials

ORIGINAL RESEARCH
published: 07 May 2021
doi: 10.3389/fmats.2021.683851

Analysis of Anomalous Dynamic Responses of Fiber Metal Laminates Under Pulse Loading

Hongbo Zhai[1], *Jianwei Zhu*[2], *Boyong Mao*[1] *and Wenyang Liu*[2]*

[1]*Xi'an Modern Chemistry Research Institute, Xi'an, China,* [2]*College of Mechanical and Vehicle Engineering, Hunan University, Changsha, China*

Composed of metallic layers and composite plies, fiber metal laminates (FMLs) combine inherent advantages of metals and composites. The phenomenon of anomalous response behavior, in which the permanent deformation is in the opposite direction to the incoming pressure wave, has been discovered in dynamic responses of monolithic plate subjected to impulsive loading. In this study, dynamic responses of FML plates of various configurations are examined and compared against the responses of a monolithic plate using finite element analysis. It is found that under the load condition in which an anomalous dynamic behavior of an aluminum plate is observed, FMLs oscillate a few cycles before resting on permanent deformation, and the laminate thickness strongly affects the final deflection, which could be in the counter-intuitive direction or near the initial position of zero deflection depending on configuration and specification of FMLs. In addition, interaction of damage accumulation with deflection responses is investigated. The findings of this study can be useful for optimal design of FMLs intended for usage under extreme loadings.

Keywords: Composites, FML, dynamic responses, impulsive loads, damage evolution

OPEN ACCESS

Edited by:
Ping Xiang,
Central South University, China

Reviewed by:
Rulin Shen,
Central South University, China
Fei Han,
Dalian University of Technology, China
Zhanqi Cheng,
Zhengzhou University, China

***Correspondence:**
Wenyang Liu
liuwenyang@hnu.edu.cn

Specialty section:
This article was submitted to Structural Materials, a section of the journal Frontiers in Materials

Received: *22 March 2021*
Accepted: *21 April 2021*
Published: *07 May 2021*

Citation:
Zhai H, Zhu J, Mao B and Liu W (2021) Analysis of Anomalous Dynamic Responses of Fiber Metal Laminates Under Pulse Loading. Front. Mater. 8:683851. doi: 10.3389/fmats.2021.683851

INTRODUCTION

Composite materials are composed of two or more different substances, each with its own characteristics, combined to achieve superior properties than the constituent materials (Lapczyk and Hurtado, 2007; Guo et al., 2021). Having witnessed a rapidly development, composite materials are widely used in erospace, automotive, electrical, construction, and other fields (Ameri, Moradi and Talebitooti, 2020; Wanchoo et al., 2021). Active research on the dynamic behavior of composite materials includes rate dependence of mechanical properties (Wang et al., 2021), constitutive models (Zhan et al., 2021), damage evolution such as shear softening upon dynamic loading (Tang et al., 2017), and etc.

Fiber-metal laminates (FMLs) are made of thin metal layers alternating with composite layers having a unidirectional, cross-ply, or fabric structure (Vasiliev and Morozov, 2018). FMLs combine advantages of fiber-reinforced composite materials and metals, possessing high specific strength, fatigue resistance, and excellent impact resistance (Andrew et al., 2019; Nicolinco et al., 2021). A particular important application of FMLs is using them in conditions that involving severe and extreme loads to absorb energies (Sasso et al., 2019; Jia et al., 2021). The dynamic responses of FMLs under various loading conditions have drawn research interest. One category is the study of projectile impacts, including FMLs under low-speed and high-speed projectile impacts (Lee et al., 2018; Li et al., 2018; Sharma et al., 2021), multiple impacts with the same total energy (Yao et al., 2019), the influence of projectile deformability (Sangsefidi et al., 2021), and etc.

Impulsive loading is characterized by high intensity and short duration. While metal plates made of aluminum alloys or steel (Chen and Hao, 2014; Micallef et al., 2016; Cerik, 2017; Zhang et al., 2020), stiffened structures (Zhao et al., 2020; Fu et al., 2021; Kong et al., 2021), as well as other innovative forms of structures (Sun et al., 2019; Zhou and Jing, 2020; Jing et al., 2021) under impulsive loads have been intensively studied, FMLs subjected to intensive short duration loading, however, are far from being well understood. The involved complexities include the wide range of changes in strain rate under blast loading (Zhang et al., 2018; Xu et al., 2020), interaction of fragments with blast waves (Dhari, 2021), modeling of interfacial debonding between adjacent plies (Soutis et al., 2011), and sensitivity to the load characteristics (Karagiozova et al., 2010).

Anomalous dynamic responses, also knowns as counter-intuitive behaviors, have been found in ductile metal objects subjected to a pressure pulse. The final deflections are in the direction opposite to that of the pressure applied during the pulse. Since the discovery of this interesting dynamic behavior (Symonds and Yu, 1985), theoretical, experimental, and numerical studies have been conducted on the counter-intuitive behavior of beams and plates under impact and impulse loads. It has been realized that the counter-intuitive behavior is related with the elastic-plastic non-linearity and the compressive instability (Dong et al., 2011). Under impulsive loading conditions, the negative phase due to the momentum of air that generates an overexpansion has been found to have significant influence on the occurrence of counter-intuitive behaviors (Aune et al., 2016). Attention to counter-intuitive behavior is deserved because it is an unstable configuration that a small loading less than the failure level might leads to catastrophic results (Ma et al., 2015). However, the responses of FMLs are not clear in the dynamically anomalous regime that has been observed for monolithic metal plates. Hence, unexpected but potentially disastrous consequences of counter-intuitive behavior can be a critical factor restricting extensive usage of FMLs.

In this study, dynamic responses of FML plates subjected to impulsive loads are investigated, with special focus to anomalous response behavior. First, dynamic responses of a monolithic metal plate are studied and validated. Then, same impulsive loading conditions are applied to FML plates of varying configurations. The differences between monolithic and FML plates are examined. Lastly, the damage induced during the dynamic responses is investigated, and implications on FML design and structural applications are discussed. *Materials and Methods* is devoted to description devotes to the materials and modeling considerations. In *Results and Discussions*, numerical results are discussed. Conclusions are summarized in *Conclusion*.

MATERIALS AND METHODS

In this study, FMLs are composed of two thin aluminum layers bonded with fiber composite layers. A coding system denoted by $t_1/t_2\,[\theta_1/\theta_2]/t_3$ is adopted. For example, 0.22/0.36[0°/90°]/0.22 indicates that the bottom and top aluminum layers are of a thickness $t_1 = t_3 = 0.22$ mm and the middle composite layer is of a thickness $t_2 = 0.36$ mm with two plies of unidirectional fibers laid orthogonally to one another [0°/90°] with the angle $\theta = 0^{\circ}$ parallel to the x-axis.

In the present study, three types of FML panels with varying layer thickness and fiber orientation are studied as shown in **Figure 1**. The thickness versus weight trade-off is always an important consider in FML applications. Thus, the total thickness is set to the same value for all FML panels; the performance of different FML configurations can then be evaluated.

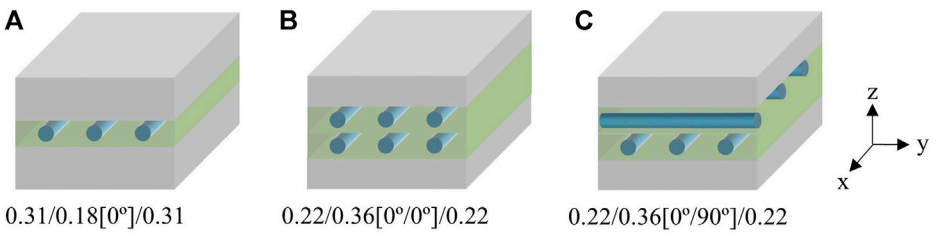

FIGURE 1 | Schematics of FMLs with varying layer thickness and fiber orientation for **(A)** 0.31/0.18[0°]/0.31 **(B)** 0.22/0.36[0°/0°]/0.31 and **(C)** 0.22/0.36[0°/90°]/0.31.

TABLE 1 | Material parameters of fiber-reinforced composites (Lapczyk and Hurtado, 2007).

Elastic properties		Failure stresses		Fracture energies		Viscosity coefficients	
E_{11} (MPa)	55,000	X^T (MPa)	2,500	G_{ft}^c (N/mm)	12.5	η_{ft}	0.001
E_{22} (MPa)	9,500	X^C (MPa)	2000	G_{fc}^c (N/mm)	12.5	η_{fc}	0.001
ν_{12}	0.33	Y^T (MPa)	50	G_{mt}^c (N/mm)	1	η_{mt}	0.005
G_{12} (MPa)	5,500	Y^C (MPa)	150	G_{mc}^c (N/mm)	1	η_{mc}	0.005
G_{13} (MPa)	3,000	S^L (MPa)	50				
G_{23} (MPa)	3,000	S^T (MPa)	75				

Dynamic responses of FML plates subjected to impulsive loads are studied via numerical simulations. The plate dimensions are $300 \times 300 \times 0.8\ mm^3$, and edges are fully constrained in the finite element simulations to model clamped boundary conditions. The density of aluminum is $2.7\ g/cm^3$, the Young's modulus is 70 GPa, the Poisson's ratio is 0.33, and the specific heat capacity is $910J/(kg \cdot K)$, and the material properties of the fiber-reinforced composite are shown in **Table 1**.

Metal Constitutive Relation

In order to simulate large elastoplastic deformation of metal, the rate of deformation is decomposed into elastic and plastic parts as

$$D = \boldsymbol{D}^{\mathrm{e}} + \boldsymbol{D}^{P} \tag{1}$$

where $\boldsymbol{D}^{\mathrm{e}}$ is the elastic deformation rate, and $\boldsymbol{D}^{P}$ is the plastic deformation rate. The elastic constitutive relationship is defined as

$$\boldsymbol{D}^{\mathrm{e}} = \frac{1+\nu}{E}\boldsymbol{\sigma}^{\nabla J} - \frac{\nu}{E}\mathrm{tr}\left(\boldsymbol{\sigma}^{\nabla J}\right)\boldsymbol{I} \tag{2}$$

where E is Young's modulus, ν is Poisson's ratio, $\boldsymbol{\sigma}^{\nabla J}$ is the Jaumann rate of Cauchy stress, and $\boldsymbol{I}$ is the second order identity tensor.For isotropic materials, the yield function is defined as

$$f\left(\boldsymbol{\sigma}, \varepsilon^{p}, T\right) = \sigma_{eq} - \sigma_{y}\left(\varepsilon^{p}, T\right) \tag{3}$$

where σ_{eq} is the equivalent stress, ε^{p} is the equivalent plastic strain, T is the temperature, and

$$\sigma_{eq} = \sqrt{\frac{3}{2}\boldsymbol{\sigma}' : \boldsymbol{\sigma}'} \tag{4}$$

$$\boldsymbol{\sigma}' = \sigma - \frac{1}{3}\mathrm{tr}\left(\boldsymbol{\sigma}\right)I \tag{5}$$

where $\boldsymbol{\sigma}'$ is the stress deviation, and the plastic strain increment is related to the stress deviator.The yield stress function is defined as (Aune et al., 2017).

$$\sigma_{y} = \left[\sigma_{0} + \sum_{i=1}^{2} Q_{i}\left(1 - \exp\left(-C_{i}\varepsilon^{p}\right)\right)\right]\left[1 + \frac{\dot{\varepsilon}^{p}}{\dot{\varepsilon}_{0}^{p}}\right]^{c}\left[1 - T^{*m}\right] \tag{6}$$

where σ_0 is the initial yield stress, Q_1, Q_2, C_1, C_2 are the material hardening parameters, $\dot{\varepsilon}_{0}^{p}$ is the reference plastic strain rate, and the expression of T^* is given as

$$T^{*} = \frac{T - T_{r}}{T_{m} - T_{r}} \tag{7}$$

where T_r is the ambient temperature, and T_m is the melting temperature of the material. Assuming that the plastic potential function coincides with the yield function, the plastic deformation rate tensor can be expressed as

$$\boldsymbol{D}^{P} = \dot{\varepsilon}^{p}\frac{\partial f}{\partial \boldsymbol{\sigma}} = \frac{3}{2}\dot{\varepsilon}^{p}\frac{\boldsymbol{\sigma}'}{\sigma_{eq}} \tag{8}$$

Since materials undergo rapid plastic deformation subjected to impulsive loads, the adiabatic process is assumed. The rate of temperature rise is defined as

$$\dot{T} = \frac{\chi}{\rho C_{p}}\sigma : \boldsymbol{D}^{p} = \frac{\chi}{\rho C_{p}}\sigma_{eq}\dot{\varepsilon}^{p} \tag{9}$$

where χ is the Taylor-Quinney coefficient, ρ is the density, and C_p is the specific heat. The material parameters used in the metal constitutive relation are shown in **Table 2**.

Modeling of Fiber Reinforced Polymer

Because of geometrical feature of the FML plates having a thickness significantly smaller than the other dimensions, the aluminum and composites layers are modeled using shell elements. Composite layups can be composed of plies made of different materials in different orientations. To simplify the model, the shell composite layup model in ABAQUS that discretizes only the reference surfaces for each ply is used, and thus fibers and matrix are not explicitly modeled.

The failure criteria of fiber-reinforced composite materials adopt the Hashin's theory (Hashin and Rotem, 1973; Hashin, 1980) that has been implemented in the commercial finite element package ABAQUS. Four different modes of failure are considered including fiber rupture in tension, fiber buckling and kinking in compression, matrix cracking under transverse tension and shearing, and matrix crushing under transverse compression and shearing. The initiation criterion is expressed as

$$d_{f} = \begin{cases} \left(\dfrac{\widehat{\sigma}_{11}}{X^{T}}\right)^{2} + \alpha\left(\dfrac{\widehat{\tau}_{12}}{S^{L}}\right)^{2}, & \widehat{\sigma} \geq 0 \\ \left(\dfrac{\widehat{\sigma}_{11}}{X^{C}}\right)^{2}, & \widehat{\sigma}_{11} < 0 \\ \left(\dfrac{\widehat{\sigma}_{22}}{Y^{T}}\right)^{2} + \left(\dfrac{\widehat{\tau}_{12}}{S^{L}}\right)^{2}, & \widehat{\sigma}_{22} \geq 0 \\ \left(\dfrac{\widehat{\sigma}_{22}}{2S}\right)^{2} + \left[\left(\dfrac{Y^{C}}{2S^{T}}\right)^{2} - 1\right]\dfrac{\widehat{\sigma}_{22}}{Y^{C}} + \left(\dfrac{\widehat{\tau}_{12}}{S^{L}}\right)^{2}, & \widehat{\sigma}_{22} < 0 \end{cases}$$

where X^T denotes the longitudinal tensile strength, X^C denotes the longitudinal compressive strength, Y^T denotes the transverse tensile strength, Y^C denotes the transverse compressive strength, S^L denotes the longitudinal shear strength, S^T denotes the transverse shear strength, α is a coefficient that determines the contribution of the shear stress to the fiber tensile initiation criterion, and $\widehat{\sigma}_{11}$, $\widehat{\sigma}_{22}$, $\widehat{\tau}_{12}$ are components of the effective stress tensor. A value of $d_f \geq 1.0$ indicates that the initiation criterion has been met.

When damage begins to accumulate, each failure mode has its own damage evolution and a damage index in the range of 0–1 as the measure of damage. Using the energy-based linear damage evolution law, the fracture energies G_{ft}^{c}, G_{fc}^{c}, G_{mt}^{c} and G_{mc}^{c} associated with the energy consumed in the damage process of each mode, are set in the simulations. In addition, material models with stiffness degradation usually lead to difficulties in

TABLE 2 | Material parameters for the metal constitutive relation (Aune et al., 2017).

σ_0 (MPa)	Q_1 (MPa)	C_1	Q_2 (MPa)	C_2	c	m	$\dot{p}_0\ (s^{-1})$
80.0	49.3	1,457.1	5.2	121.5	0.014	1.0	5×10^{-4}

the convergence of analyses, so the viscosity regularization scheme is used to facilitate convergence. Viscosity coefficients, η_{ft}, η_{fc}, η_{mt} and η_{mc} for each damage mode, are summarized in **Table 1**.

Modeling Considerations for Adhesive Layers

The degradation of bonding adhesive layer between metal and composite layers in an FML significantly reduce the rigidity and eventually lead to interlaminar delamination. Thus, the adhesive behavior of bonded neighboring layers must be taken into consideration. In this study, the surface-based cohesive behavior model available in ABAQUS is used.

The linear elastic traction-separation behavior is assumed in the surface-based cohesive model. Material properties used to define the elastic behavior of adhesive are summarized in **Table 3**. The debonding process consists of three phases, i.e., damage initiation, damage evolution and complete failure. This study uses the quadratic separation criterion to characterize damage initiation represented as

$$\left\{\frac{\langle\delta_n\rangle}{\delta_n^0}\right\}^2+\left\{\frac{\delta_s}{\delta_s^0}\right\}^2+\left\{\frac{\delta_t}{\delta_t^0}\right\}^2=1,\ \langle\delta_n\rangle=\begin{cases}\delta_n & \delta_n>0\\ 0 & \delta_n<0\end{cases} \tag{11}$$

where δ_n^0, δ_s^0, and δ_t^0 represent the values of separation, when the separation is either purely along the contact normal or purely in the first or the second shear direction, respectively. δ_n, δ_s, and δ_t represent distances of separation in different directions.

The law of damage evolution describes the degradation rate of stiffness once the initiation criterion is reached. The energy-based exponential damage evolution law is adopted, and the power law criterion is used to describe the interaction of mixed modes as (Camanho and Davila, 2002)

$$\left\{\frac{G_n}{G_n^C}\right\}^2+\left\{\frac{G_s}{G_s^C}\right\}^2+\left\{\frac{G_t}{G_t^C}\right\}^2=1 \tag{12}$$

where G_n^C, G_s^C and G_t^C refer to the critical fracture energies required to cause failure in the normal, the first, and the second shear directions, respectively. G_n, G_s and G_t represent the work done by the tractions and their conjugate separations. The mixed-mode fracture energy is

$$G^C=\frac{1}{\left(\left\{\frac{m_1}{G_n^C}\right\}^\alpha+\left\{\frac{m_2}{G_s^C}\right\}^\alpha+\left\{\frac{m_3}{G_t^C}\right\}^\alpha\right)^{\frac{1}{\alpha}}} \tag{13}$$

where $m_1=G_n/G_T$, $m_2=G_s/G_T$, $m_3=G_t/G_T$, and $G_T=G_n+G_s+G_t$. Exponential softening is expressed by the evolution of damage variable D as

$$D=\int_{\delta_m^0}^{\delta_m^f}\frac{T_{\text{eff}}}{G^C-G_0}d\delta \tag{14}$$

where δ_m^f denotes the displacement at complete failure, δ_m^0 denotes the displacement at the beginning of the damage, T_{eff} and δ are the traction and separation, respectively, and G_0 is the elastic energy at damage initiation.

Modeling of Impulsive Loading

A primary goal of this study is to investigate the anomalous dynamic response that is highly sensitive to the applied loads, hence the load function is of critical importance. While many studies use simplified pulse shapes such as triangles or rectangles in their numerical simulations, an in-house code specifically developed for modeling the impulsive pressure is ported to commercial finite element software via user defined subroutines in the present study.

The pressure-time history is comprised of positive and negative phases as shown in **Figure 2**. The pressure profile is characterized by the ambient pressure p_0, peak reflected overpressure $p_{r\alpha}$ with the subscript α denoting the angle of incidence, negative overpressure $p_{r,\min}$, arrival time t_a, positive duration t_d^+, negative duration t_d^-, and decay parameter b.

The required input parameters for the impulsive load function are the location of source and equivalent charge weight. The scaled distance using the Hopkinson-Cranz scaling law can be used to describe the intensity of shock loading as

$$Z=\frac{R}{W^{\frac{1}{3}}} \tag{15}$$

where R is the stand-off distance and W is the equivalent weight. The positive phase of the pressure-time history can be described by the modified Friedlander equation expressed as

$$p(t)=p_0+p_{r\alpha}\left(1-\frac{t-t_a}{t_d^+}\right)\exp\left(\frac{-b(t-t_a)}{t_d^+}\right)\qquad t_a<t<t_a+t_d^+ \tag{16}$$

The reflected pressure considering the angle of incidence α can be calculated by

$$p_{r\alpha}=p_{\text{inc}}\left(1+\cos\alpha-2\cos^2\alpha\right)+p_{\text{ref}}\cos^2\alpha$$

where p_{inc} and p_{ref} are incidence and reflected pressures, respectively. By integrating the positive phase of pressure over time, the impulse i_r^+ is obtained

$$\begin{aligned}i_{r\alpha+}&=\int_{t_a}^{t_a+t_d^+}p_{r\alpha}\left(1-\frac{t-t_a}{t_d^+}\right)\exp\left(\frac{-b(t-t_a)}{t_d^+}\right)\\&=\frac{p_{r\alpha}t_d^+}{b^2}\left(b-1+\exp(-b)\right)\end{aligned} \tag{17}$$

Since p_{inc}, p_{ref}, $i_{r\alpha+}$ are given as functions of the stand-off distance R and weight W, the decay parameter b can be implicitly solved.

TABLE 3 | Material parameters for cohesive behavior (Lapczyk and Hurtado, 2007).

E (MPa)	G_1 (MPa)	G_2 (MPa)	ε_n^0	ε_s^0	ε_t^0	G_n^C (N/mm)	G_s^C (N/mm)	G_t^C (N/mm)
2000	752	752	0.025	0.067	0.067	4	4	4

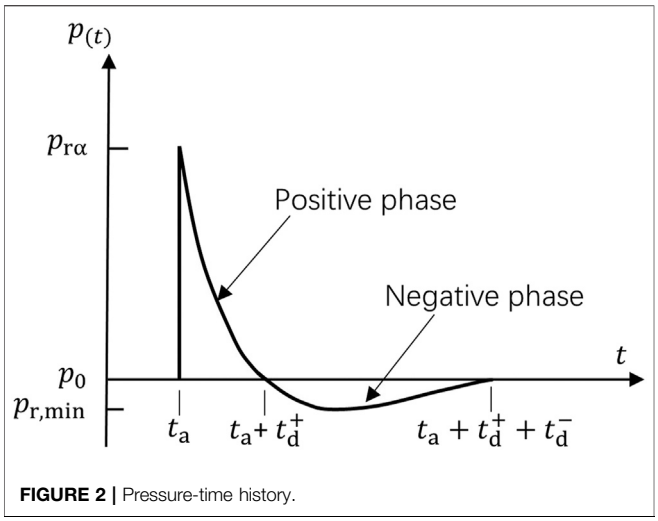

FIGURE 2 | Pressure-time history.

The negative phase of the pressure is critical to the occurrence of counter-intuitive behavior; thus, it must be considered in the loading function. A bilinear approximation of the negative phase is adopted (Aune et al., 2017), and the full expression of pressure is defined as

$$p(t) = \begin{cases} p_0, & t < t_a \\ p_0 + p_{r\alpha}\left(1 - \frac{t - t_a}{t_d^+}\right)\exp\left(\frac{-b(t - t_a)}{t_d^+}\right), & t_a < t < t_a + t_d^+ \\ p_0 - p_{r,min}\left(\frac{t - (t_a + t_d^+)}{ct_{d,lin-}}\right), & t_a + t_d^+ < t < t_a + t_d^+ + at_{d,lin-} \\ p_0 - p_{r,min}\left(\frac{t - (t_a + t_d^+ + ct_d^-)}{(1-c)t_d^-}\right), & t_a + t_d^+ + at_{d,lin-} < t < t_a + t_d^+ + t_{d,lin-} \\ p_0, & t > t < t_a + t_d^+ + t_{d,lin-} \end{cases} \quad (18)$$

Where t_d^- is the time duration of negative phase, which is typically longer than that of the positive phase, and the coefficient c is introduced to control the proportion of the negative pressure rise time in the entire negative pressure duration.

RESULTS AND DISCUSSIONS

Dynamic Response of a Monolithic Metal Plate

In this subsection, the dynamic response of an aluminum plate under impulsive loading is studied and compared against experimental results available in literature. The dimensions of the plate are $300 \times 300 \times 0.8$ mm^3 with edges fully clamped. Two impulsive loads of varying intensity defined in terms of the Hopkinson-Cranz scaled distance, $Z = 1.46$ m/kg$^{1/3}$ and $Z = 1.82$ m/kg$^{1/3}$, are considered.

The deflection at the plate center is shown in **Figure 3**, indicating radically different dynamic responses of the plate subjected to impulsive loads of varying intensity. The final deflection of the plate under the impulsive load of $Z = 1.46$ m/kg$^{1/3}$ is around 25 mm. On the other hand, the impulsive load of $Z = 1.82$ m/kg$^{1/3}$ yields a negative final deflection around -20 mm with the plate resting on the opposite direction to the incoming impulsive load. This phenomenon is referred to as anomalous or counter-intuitive behavior. **Figure 4** shows the final configurations of the plate. Different signs in the out-of-plane (i.e., the z-direction) displacement can easily be noticed. The predicted permanent deflections are validated against the experimental results reported in (Aune et al., 2016). Good agreement between numerical predictions and experiments is reached. It must be emphasized that since the counter-intuitive behavior only occurs in a tight range of impulsive loads, the accuracy of loading function is crucial to the prediction of counter-intuitive behavior. A slight discrepancy might lead to wrong results in predictions of anomalous responses. Consistency with the experimental results in both intuitive and counter-intuitive behaviors underpins the following studies of FMLs subjected to impulsive loading.

Dynamic Responses of Fiber-Metal Laminate Plates

We then study dynamic responses of FML plates and examine the difference in comparison to the responses of the monolithic metal plate. The geometries and material

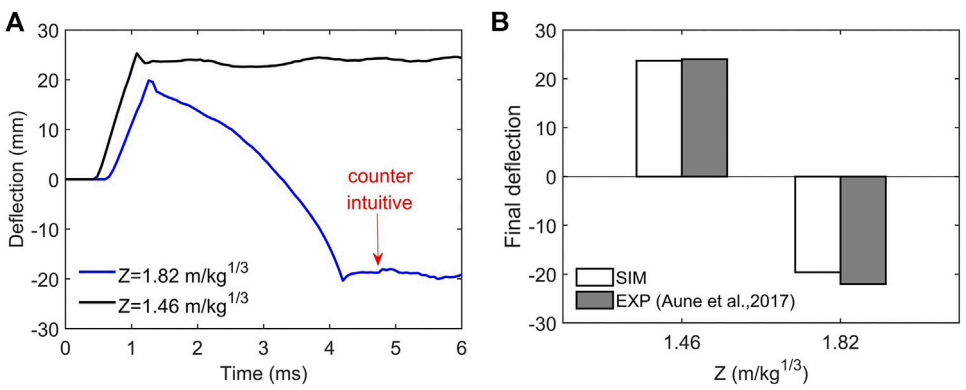

FIGURE 3 | Dynamic responses of a monolithic metal plate. **(A)** The deflection time histories at the plate center. **(B)** The final deflections under two impulsive loads defined in terms of the scaled distance ***Z***.

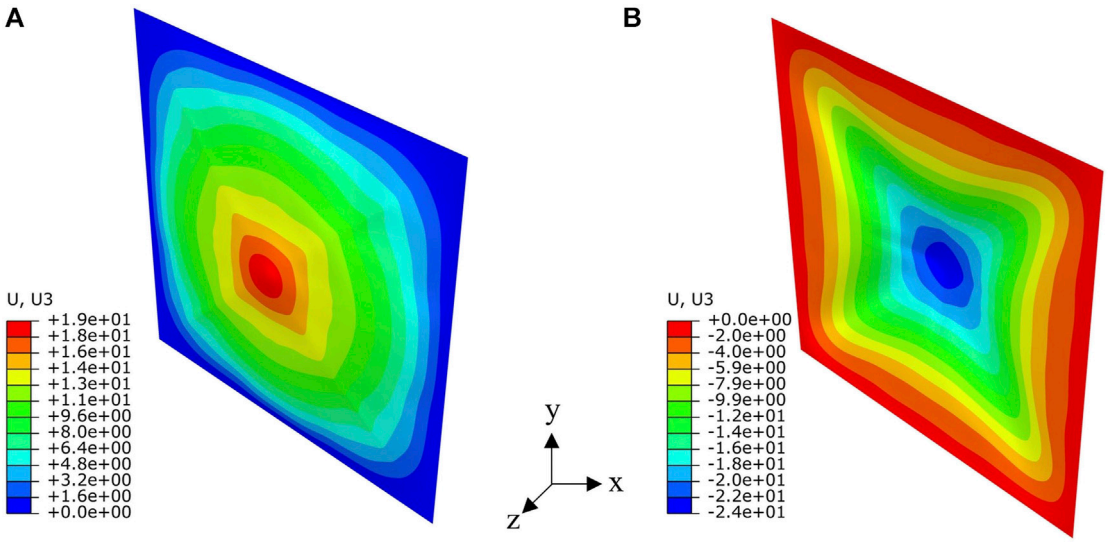

FIGURE 4 | Final permantent deformation of metal plate subjected to impulsive loads of **(A)** $\boldsymbol{Z}$ = 1.82 $\mathbf{m/kg^{1/3}}$ that leads to an counter-intuitive behavior and **(B)** $\boldsymbol{Z}$ = 1.46 $\mathbf{m/kg^{1/3}}$ that leads to intuitive deformation.

properties have been summarized in *Materials and Methods*. The thickness of the FML plates under consideration is identical to that of the aluminum plate studied in *Dynamic Response of a Monolithic Metal Plate*, so a quantitative comparison in dynamic responses can be made between monolithic and FML plates.

Figure 5A plots the deflection time histories at the plate center with the impulsive load of Z = 1.82 m/kg$^{1/3}$. Once reaching the maximum positive deflection, all three FML plates rebound toward the opposite direction to the incoming impulsive load. After about two cycles of oscillation from the lowest negative deflection, FML plates progressively arrive at their final configuration. Like the monolithic aluminum plate, the FML plate with a 0.18 mm composite layer reaches a final configuration with a negative deflection at the plate center. But the deflection is reduced by 42% from 19.16 mm to 11.20 mm. Two FML plates with a 0.22 mm composite layer approach their initial configuration of zero deflection at the plate center. What stands out in **Figure 5B** is that the thickness of composite layer in an FML only mildly affects the maximum positive deflection but imposes a strong effect on the final configuration.

Figure 6 shows the final deformation profiles of FML plates. For the 0.31/0.18[0°]/0.31 FML plate, the deformation profiles along the x- and y-directions demonstrate a significant difference due to the directionality of composite layer. On the other hand, the FML with two orthogonally laid plies of fibers, i.e., the 0.22/0.36[0°/90°]/0.22 plate, demonstrate a much smaller difference in the deformation profiles along the x- and y-directions. More importantly, the slope of the y-direction

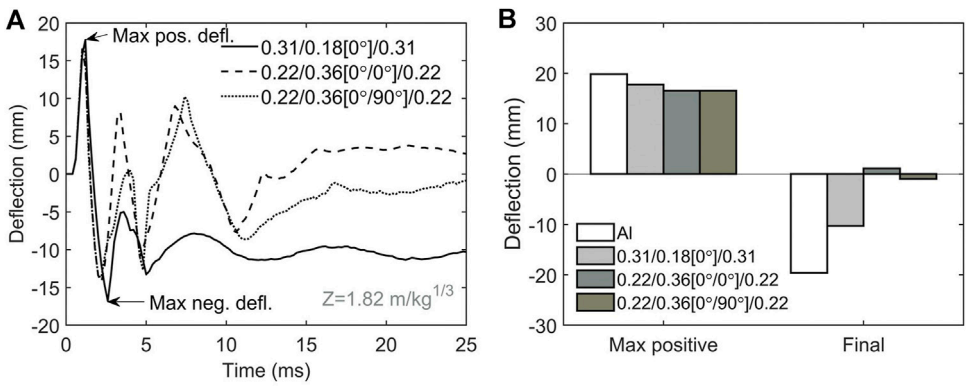

FIGURE 5 | Dynamic responses of FML plates under the impulsive load of $\boldsymbol{Z}$ = 1.82 $\mathbf{m/kg^{1/3}}$. **(A)** The deflection time histories at the plate center. **(B)** Comparison of maximum positive deflection and final deflection between aluminum and FML plates.

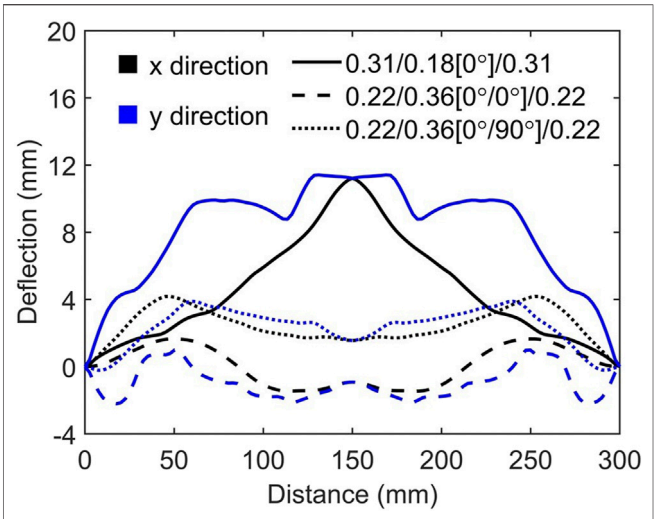

FIGURE 6 | The final deformation profiles of FML plates under the impulsive load of $\boldsymbol{Z}$ = 1.82 $\mathbf{m/kg^{1/3}}$.

deformation profile near the edge is considerably higher in the FML plate with only unidirectional lamina. As large deflection slope might eventually lead to tearing of the plate at the boundary, special attention in structural design is thus desired.

Given the considerable difference in the slope of deflection near the plate edges, we further inspect the state of stress triaxiality defined as the ratio of the hydrostatic mean stress to the von Mizes equivalent stress, i.e., $\sigma^* = \sigma_H/\sigma_{eq}$ in which the hydrostatic mean stress defined in terms the principal stresses as $\sigma_H = (\sigma_1 + \sigma_2 + \sigma_3)/3$. It is generally accepted that shear fracture is the failure mechanism in the negative stress triaxiality regime and fracture due to void formation in the high stress triaxiality regime (Bao and Wierzbicki, 2004). **Figure 7A** plots the evolution of stress triaxiality at the mid-point of edge perpendicular to the fiber direction. Upon the arrival of pressure pulse, the stress triaxiality abruptly increases to a state of 0.6 in the vicinity of the top cohesive interface, and a negative stress triaxiality of −0.4 is reached near the bottom interface. During the dynamic responses to the impulsive loading, the stress triaxiality intensely oscillates between positive and negative regimes, indicating different failure mechanisms can be activated once a threshold value, such as critical strain, is reached. When the plate eventually rests on its final configuration, the stress triaxialities are positive on the top and negative on the bottom interfaces, respectively. **Figure 7B** shows the evolution of stress triaxiality at the mid-point of edge parallel to the fiber direction. Positive stress triaxialities develop near both top and bottom cohesive interfaces upon the arrival of pressure pulse. Two phases of oscillation in triaxiality are noticed, first in the range of 0.6 to −0.6 and −0.2 to −0.6 subsequently. When the plate rests on its final configuration, the stress triaxialities are negative on the top and positive on the bottom interfaces, respectively. The clear differences in the state of stress triaxiality observed in **Figures 7A,B** is closely related with the fiber orientation.

Next, we examine the dynamic responses of FML plates subjected to higher intensity of impulsive loading with the scaled distance Z = 1.46 m/kg$^{1/3}$. **Figure 8** shows the deflection versus time at the plate center. Recall that the permanent displacement of the aluminum plate is in the intuitive direction under the impulsive load of Z = 1.46 m/kg$^{1/3}$ (see **Figure 3**). The 0.31/0.18 [0°]/0.31 plate, however, demonstrate a counter-intuitive behavior with the permanent deflection in the opposite direction to the incident impulsive loading. Hence, it is inferred that the dynamic responses of monolithic and FML plates can be entirely different. Furthermore, unlike the 0.31/0.18 [0°]/0.31 plate, both 0.22/0.36 [0°/0°]/0.22 and 0.22/0.36 [0°/90°]/0.22 plates demonstrate an intuitive permanent deformation with positive deflection at the plate center, suggesting significant influences of FML configurations on dynamic responses. The presence or absence of counter-intuitive behavior is affected by many factors, such as material properties (Li et al., 2008), load magnitudes and profiles (Symonds and Yu, 1985; Aune et al., 2017), boundary conditions (Bassi et al., 2003), etc. The ultimate state is extremely sensitive to the initial conditions (Ng and Daolin, 2002). The analyses in the present study highlight additional, but potentially enormous, intricacy induced by

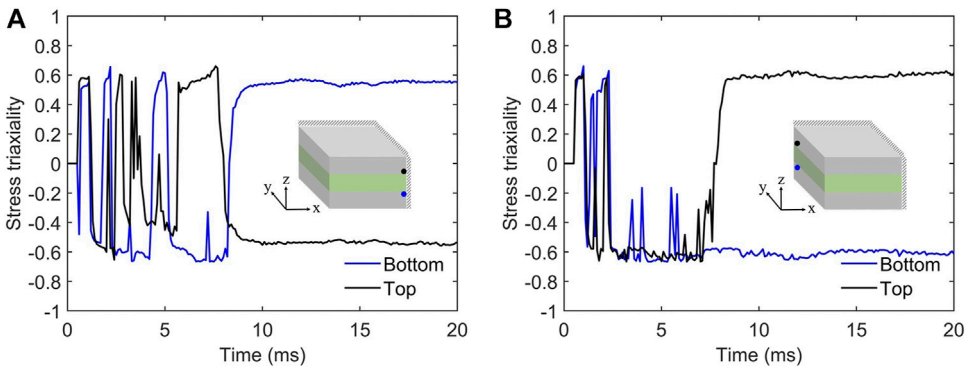

FIGURE 7 | The evolution of stress triaxiality of the 0.22/0.36 [0°/0°]/0.22 plate under the impulsive load of $\boldsymbol{Z}$ = 1.82 $\mathbf{m/kg^{1/3}}$ at **(A)** the mid-point of edge perpendicular to the fiber direction and **(B)** the mid-point of edge parallel to the fiber direction.

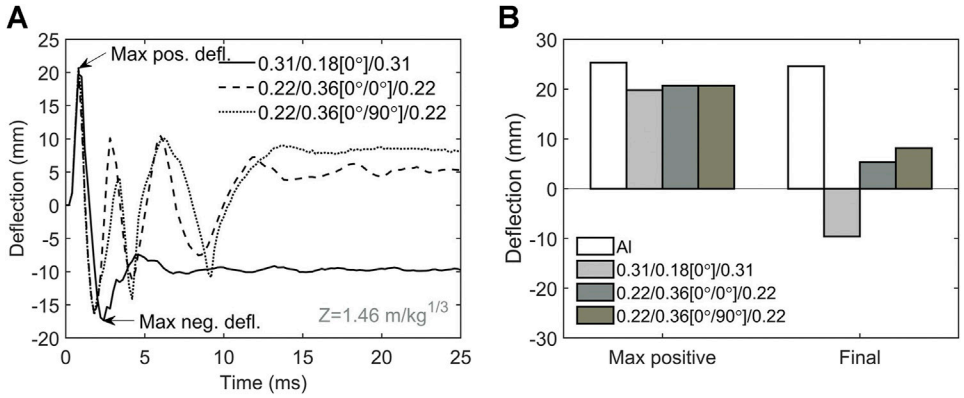

FIGURE 8 | Dynamic responses of FML plates under the impulsive load of $\boldsymbol{Z}$ = 1.46 $\mathbf{m/kg^{1/3}}$. **(A)** The deflection time histories at the plate center. **(B)** Comparison of maximum positive deflection and final deflection between aluminum and FML plates.

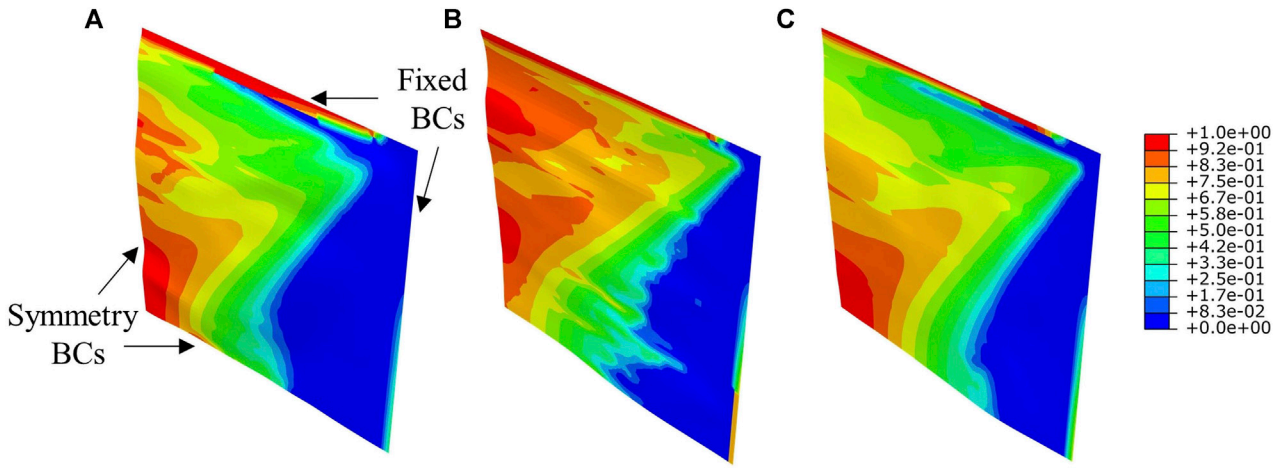

FIGURE 9 | Matrix tension damage of the composite layer under the impulsive load of $\boldsymbol{Z}$ = 1.82 $\mathbf{m/kg^{1/3}}$. **(A)** 0.31/0.18[0°]/0.31 plate. **(B)** 0.22/0.36[0°/0°]/0.22 plate. **(C)** 0.22/0.36[0°/90°]/0.22 plate. Only a quarter of the plate is illustrated with boundary conditions specified.

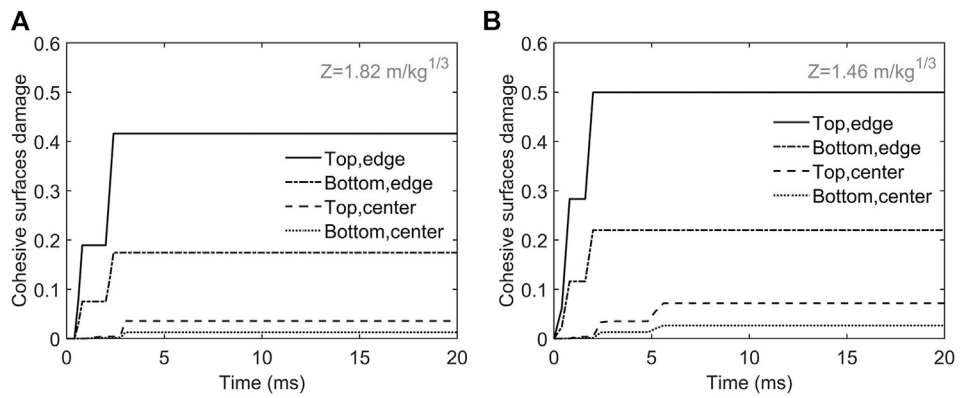

FIGURE 10 | The damage evolution at various locations of the 0.22/0.36 [0°/0°]/0.22 plate. **(A)** With the impulsive load of $\boldsymbol{Z}$ = 1.82 $\mathbf{m/kg^{1/3}}$. **(B)** With the impulsive load of $\boldsymbol{Z}$ = 1.46 $\mathbf{m/kg^{1/3}}$.

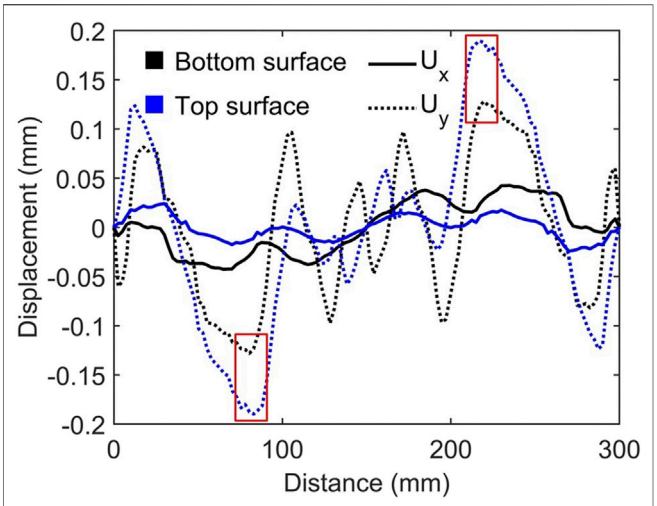

FIGURE 11 | The displacements along the x- and y-centerlines of the 0.22/0.36 [0°/0°]/0.22 plate under the impulsive load of $\boldsymbol{Z}$ = 1.46 **m/kg**$^{1/3}$.

FMLs to the nonlinear responses that deserve attention in structural design and applications.

Damage of Fiber-Metal Laminate Plates

For all three FML plates subjected to the scaled pulse Z = 1.82 m/kg$^{1/3}$, composite layers suffer matrix tension damage as shown in **Figure 9**. Comparing **Figures 9A,B** reveals the influence of the ratio of the metal to composite layer thickness while the total plate thickness is kept the same for both cases. It is found that the 0.31/0.18[0°]/0.31 plate suffers less damage than the 0.22/0.36[0°/0°]/0.22 plate. Therefore, a thicker aluminum layer attenuates the matrix damage resulted from impulsive loading. Additionally, reducing aluminum layer thickness tends to shift damage from the plate center to the edges along the direction perpendicular to the fiber direction as shown in **Figure 9B**. Two orthogonally laid plies have a beneficial effect in reducing damage as shown in **Figure 9C**. In general, the plate center and clamping edges are of high propensity to accumulate damage. To further reduce the extent of damage, the thickness of the FML plates needs to increase.

The degradation and eventual failure of bonding between two cohesive surfaces are major concerns for applications using FMLs. **Figure 10** shows the damage evolution at various locations of the 0.22/0.36 [0°/0°]/0.22 plate. Overall, the top cohesive interface, which is closer to the source of impulsive loading, suffers severer damage than the bottom cohesive interface; plate edges sustain more damage than the center, which is closer to the source though. Although damage is produced, no debonding takes place for both Z = 1.82 m/kg$^{1/3}$ and Z = 1.46 m/kg$^{1/3}$.

It is worth pointing out that although the impulsive loading is applied normal to the plate surface, localized sliding can occur between layers. To illustrate this phenomenon, the displacements along the x- and y-centerlines of the plate are plotted in **Figure 11**. A particular noteworthy finding is that localized sliding can arise at locations that are often overlooked (see the rectangle annotations in **Figure 11** The displacements along the x- and y-centerlines of the 0.22/0.36 [0°/0°]/0.22 plate under the impulsive load of Z = 1.46 m/kg$^{1/3}$.) especially if the final permanent deflection is small or even close to the zero. The localized sliding due to inconsistency in in-plane displacements might lead to fiber kinking and several other failure types (Greenhalgh, 2009).

Lastly, in order to clearly understand the damage of FML during the dynamic response, the energy dissipated by damage is plotted as shown in **Figure 12**. In the case of impulsive load Z = 1.82 m/kg$^{1/3}$, the energy dissipation due to damage is very close in value for the 0.31/0.18 [0°]/0.31 and 0.22/0.36 [0°/0°]/0.22 FML plates although the configuration of layer thickness is different; the FML plate with two plies of unidirectional fibers laid orthogonally, on the other hand, induces less damage energy. Under the condition of a higher impulsive load Z = 1.82 m/kg$^{1/3}$, the energy dissipated by damage increases to twice that of the previous load. Additionally, the difference in energy between 0.31/0.18 [0°]/0.31 and 0.22/0.36 [0°/0°]/0.22 FML plates can be noticed, suggesting a better protective performance of thicker composite layer.

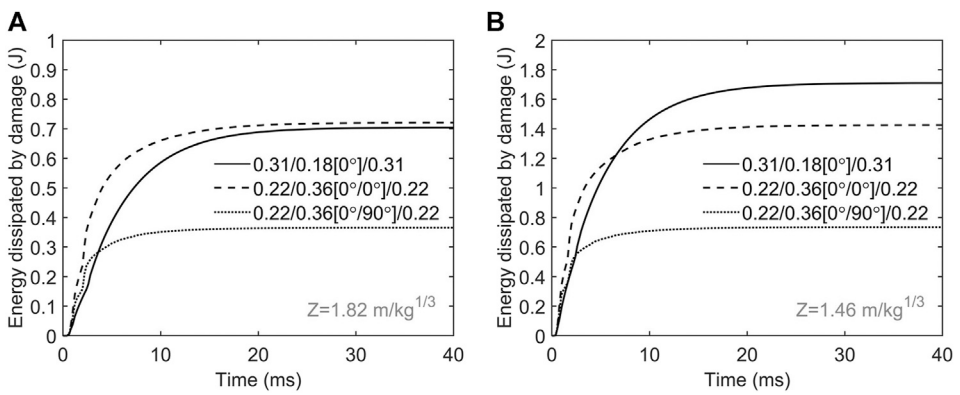

FIGURE 12 | Energy dissipated by damage with **(A)** the impulsive load of **Z** = 1.82 **m/kg**$^{1/3}$ and **(B)** the impulsive load of **Z** = 1.46 **m/kg**$^{1/3}$.

CONCLUSION

Dynamic responses of FML plates subjected to impulsive loads are investigated, with special focus to anomalous response behavior. Modeling considerations include high strain-rate ductile plasticity, failure criteria for fiber reinforced polymer, degradation of adhesive layers, and validated pressure pulses that strongly affect predictions of counter-intuitive behaviors under impulsive loadings. Different FML configurations under impulsive loadings are examined.

First, dynamic responses of a monolithic plate made of aluminum are examined. A counter-intuitive behavior with the final permanent deflection in the opposite direction to the incoming load is predicted numerically. This anomalous behavior vanishes as the loading intensity, which is characterized by the scaled distance, decreases by 20%. The numerical predictions are validated against experimental results available in literature.

Under the same loading conditions, dynamic responses of FML plates of different configurations are studied. Remarkably different responses are noticed. While the maximum positive deflections of FML plates are consistently reduced in all cases, the final permanent deformation shows a wide disparity among FML configurations and load intensities. Under the load condition in which an anomalous dynamic behavior of the aluminum plate is observed, FMLs oscillate before resting on permanent deformation, and the laminate configuration and specification strongly affect the final deflection, which might hold position in the counter-intuitive direction opposite to the incoming pulse or in the vicinity of the initial position with small permanent deflection. Interestingly, after decreasing the scaled distance such that the anomalous behavior vanishes for the aluminum plate, a counter-intuitive behavior still exists in the FML plate that has a thinner composite layer than the other FML plates.

On one hand, the anomalous behavior is related with the elastic-plastic non-linearity and the compressive instability; on the other, interaction with damage accumulation in plates made of FMLs deserves attention. It is found that in the studied loading cases, stress triaxialities in different layers as well as along different directions are noticed to be quite different, suggesting different state of deformation such as tension or shear. Lastly, although matrix damage due to tension is the main failure mechanism in the present study, localized sliding is noticed between layers.

DATA AVAILABILITY STATEMENT

The raw data supporting the conclusions of this article will be made available by the authors, without undue reservation.

AUTHOR CONTRIBUTIONS

HZ, JZ, and WL conceived and designed the study. JZ, WL, and BM carried out the simulation work. HZ, JZ, and WL reviewed and edited the manuscript. All authors contributed to the article and approved the submitted version.

FUNDING

This work was financially supported by the Open Collaboration and Innovation Fund of Xi'an Modern Chemistry Research Institute.

REFERENCES

Ameri, B., Moradi, M., and Talebitooti, R. (2021). Effect of Honeycomb Core on Free Vibration Analysis of Fiber Metal Laminate (FML) Beams Compared to Conventional Composites. *Compos. Structures* 261 (May 2020), 113281. doi:10.1016/j.compstruct.2020.113281

Andrew, J. J., Srinivasan, S. M., Arockiarajan, A., and Dhakal, H. N. (2019). Parameters Influencing the Impact Response of Fiber-Reinforced Polymer Matrix Composite Materials: A Critical Review. *Compos. Structures* 224 (December), 111007. doi:10.1016/j.compstruct.2019.111007

Aune, V., Fagerholt, E., Hauge, K. O., Langseth, M., and Børvik, T. (2016). Experimental Study on the Response of Thin Aluminium and Steel Plates Subjected to Airblast Loading. *Int. J. Impact Eng.* 90, 106–121. doi:10.1016/j.ijimpeng.2015.11.017

Aune, V., Valsamos, G., Casadei, F., Larcher, M., Langseth, M., and Børvik, T. (2017). Numerical Study on the Structural Response of Blast-Loaded Thin Aluminium and Steel Plates. *Int. J. Impact Eng.* 99, 131–144. doi:10.1016/j.ijimpeng.2016.08.010

Bao, Y., and Wierzbicki, T. (2004). A Comparative Study on Various Ductile Crack Formation Criteria. *J. Eng. Mater. Technol. Trans. ASME* 126 (3), 314–324. doi:10.1115/1.1755244

Bassi, A., Genna, F., and Symonds, P. S. (2003). Anomalous Elastic-Plastic Responses to Short Pulse Loading of Circular Plates. *Int. J. Impact Eng.* 28 (1), 65–91. doi:10.1016/S0734-743X(02)00036-2

Camanho, P. P., and Davila, C. D. (2002). Mixed-Mode Decohesion Finite Elements for the Simulation of Delamination in Composite Materials. Washington, DC: National Aeronautics and Space Administration, Report No.: NASA/TM-2002-211737.

Cerik, B. C. (2017). Damage Assessment of Marine Grade Aluminium Alloy-Plated Structures Due to Air Blast and Explosive Loads. *Thin-Walled Structures* 110 (October), 123–132. doi:10.1016/j.tws.2016.10.021

Chen, W., and Hao, H. (2014). Experimental Investigations and Numerical Simulations of Multi-Arch Double-Layered Panels under Uniform Impulsive Loadings. *Int. J. Impact Eng.* 63, 140–157. doi:10.1016/j.ijimpeng.2013.08.012

Dhari, R. S. (2021). A Numerical Study on Cross Ply Laminates Subjected to Stray Fragments Impact Loading. *Compos. Structures* 261 (January), 113563. doi:10.1016/j.compstruct.2021.113563

Dong, Q., Li, Q. M., and Zheng, J. Y. (2011). Further Study on Counter-intuitive Response of Single-Degree-Of-Freedom Structures. *Int. J. Impact Eng.* 38 (5), 305–308. doi:10.1016/j.ijimpeng.2010.10.033

Fu, T., Zhang, M., Zheng, Q., Zhou, D., Sun, X., and Wang, X. (2021). Scaling the Response of Armor Steel Subjected to Blast Loading. *Int. J. Impact Eng.* 153, 103863. doi:10.1016/j.ijimpeng.2021.103863

Greenhalgh, E. (2009). Failure Analysis and Fractography of Polymer Composites. Chennai, TN: Elsevier. doi:10.1533/9781845696818

Guo, Q., Yao, W., Li, W., and Gupta, N. (2021). Constitutive Models for the Structural Analysis of Composite Materials for the Finite Element Analysis: A Review of Recent Practices. *Compos. Structures* 260 (August), 113267. doi:10.1016/j.compstruct.2020.113267

Hashin, Z., and Rotem, A. (1973). A Fatigue Failure Criterion for Fiber Reinforced Materials. *J. Compos. Mater.* 7 (4), 448–464. doi:10.1177/002199837300700404

Hashin, Z. (1980). 'Failure Criteria for Unidirectional Mr !'. *J. Appl. Mech.* 47 (June), 329–334. doi:10.1115/1.3153664

Jia, S., Wang, F., Zhou, J., Jiang, Z., and Xu, B. (2021). Study on the Mechanical Performances of Carbon Fiber/epoxy Composite Material Subjected to Dynamical Compression and High Temperature Loads. *Compos. Structures* 258 (December 2020), 113421. doi:10.1016/j.compstruct.2020.113421

Jing, L., Liu, K., Su, X., and Guo, X. (2021). Experimental and Numerical Study of Square Sandwich Panels with Layered-Gradient Foam Cores to Air-Blast Loading. *Thin-Walled Structures* 161 (January), 107445. doi:10.1016/j.tws.2021.107445

Karagiozova, D., Langdon, G. S., Nurick, G. N., and Chung Kim Yuen, S. (2010). Simulation of the Response of Fibre-Metal Laminates to Localised Blast Loading. *Int. J. Impact Eng.* 37 (6), 766–782. doi:10.1016/j.ijimpeng.2009.04.001

Kong, X., Zhou, H., Kuang, Z., Zheng, C., Li, X., Wu, W., et al. (2021). Corrected Method for Scaling the Dynamic Response of Stiffened Plate Subjected to Blast Load. *Thin-Walled Structures* 159, 107214. doi:10.1016/j.tws.2020.107214

Lapczyk, I., and Hurtado, J. A. (2007). Progressive Damage Modeling in Fiber-Reinforced Materials. *Composites A: Appl. Sci. Manufacturing* 38 (11), 2333–2341. doi:10.1016/j.compositesa.2007.01.017

Lee, D.-W., Park, B.-J., Park, S.-Y., Choi, C.-H., and Song, J.-I. (2018). Fabrication of High-Stiffness Fiber-Metal Laminates and Study of Their Behavior under Low-Velocity Impact Loadings. *Compos. Structures* 189 (November 2017), 61–69. doi:10.1016/j.compstruct.2018.01.044

Li, Q. M., Dong, Q., and Zheng, J. Y. (2008). Counter-intuitive Breathing Mode Response of an Elastic-Plastic Circular Ring Subjected to Axisymmetric Internal Pressure Pulse. *Int. J. Impact Eng.* 35 (8), 784–794. doi:10.1016/j.ijimpeng.2007.07.002

Li, X., Zhang, X., Guo, Y., Shim, V. P. W., Yang, J., and Chai, G. B. (2018). Influence of Fiber Type on the Impact Response of Titanium-Based Fiber-Metal Laminates. *Int. J. Impact Eng.* 114 (October 2017), 32–42. doi:10.1016/j.ijimpeng.2017.12.011

Ma, J., Fan, F., Wu, C., and Zhi, X. (2015). Counter-intuitive Collapse of Single-Layer Reticulated Domes Subject to Interior Blast Loading. *Thin-Walled Structures* 96, 130–138. doi:10.1016/j.tws.2015.08.001

Micallef, K., Fallah, A. S., Curtis, P. T., and Louca, L. A. (2016). On the Dynamic Plastic Response of Steel Membranes Subjected to Localised Blast Loading. *Int. J. Impact Eng.* 89, 25–37. doi:10.1016/j.ijimpeng.2015.11.002

Ng, T. Y., and Daolin, X. (2002). Multiple Stability and Unpredictable Outcomes in the Chaotic Vibrations of Euler Beams. *J. Vibration Acoust. Trans. ASME* 124 (1), 126–131. doi:10.1115/1.1426072

Nicolinco, C., Mahboob, Z., Chemisky, Y., Meraghni, F., Oguamanam, D., and Bougherara, H. (2021). Prediction of the Compressive Damage Response of Flax-Reinforced Laminates Using a Mesoscale Framework. *Composites Part A: Appl. Sci. Manufacturing* 140, 106153. doi:10.1016/j.compositesa.2020.106153

Sangsefidi, M., Sabouri, H., Mir, M., and Hasanpour, A. (2021). High-velocity Impact Response of Fiber Metal Laminates: Experimental Investigation of Projectile's Deformability. *Thin-Walled Structures* 159 (September), 107169. doi:10.1016/j.tws.2020.107169

Sasso, M., Mancini, E., Dhaliwal, G. S., Newaz, G. M., and Amodio, D. (2019). Investigation of the Mechanical Behavior of CARALL FML at High Strain Rate. *Compos. Structures* 222 (April), 110922. doi:10.1016/j.compstruct.2019.110922

Sharma, A. P., Velmurugan, R., Shankar, K., and Ha, S. (2021). High-velocity Impact Response of Titanium-Based Fiber Metal Laminates. Part I: Experimental Investigations. *Int. J. Impact Eng.* 152 (February), 103845. doi:10.1016/j.ijimpeng.2021.103845

Soutis, C., Mohamed, G., and Hodzic, A. (2011). Modelling the Structural Response of GLARE Panels to Blast Load. *Compos. Structures* 94 (1), 267–276. doi:10.1016/j.compstruct.2011.06.014

Sun, G., Zhang, J., Li, S., Fang, J., Wang, E., and Li, Q. (2019). Dynamic Response of Sandwich Panel with Hierarchical Honeycomb Cores Subject to Blast Loading. *Thin-Walled Structures* 142 (April), 499–515. doi:10.1016/j.tws.2019.04.029

Symonds, P. S., and Yu, T. X. (1985). Counterintuitive Behavior in a Problem of Elastic-Plastic Beam Dynamics. *J. Appl. Mech. Trans. ASME* 52 (3), 517–522. doi:10.1115/1.3169093

Tang, Y. L., Wu, R. F., Jiao, Z. M., Shi, X. H., Wang, Z. H., and Qiao, J. W. (2017). Shear Softening of Ta-Containing Metallic Glass Matrix Composites upon Dynamic Loading. *Mater. Sci. Eng. A* 704 (March), 322–328. doi:10.1016/j.msea.2017.08.046

Vasiliev, V. V., and Morozov, E. V. (2018). Advanced Mechanics of Composite Materials and Structures. Chennai, TN: Elsevier.

Wanchoo, P., Matos, H., Rousseau, C.-E., and Shukla, A. (2021). Investigations on Air and Underwater Blast Mitigation in Polymeric Composite Structures - A Review. *Compos. Structures* 263 (January), 113530. doi:10.1016/j.compstruct.2020.113530

Wang, M., Li, Y., Chen, B., Shi, D., Umeda, J., Kondoh, K., et al. (2021). The Rate-dependent Mechanical Behavior of CNT-Reinforced Aluminum Matrix Composites under Tensile Loading. *Mater. Sci. Eng. A* 808 (November 2020), 140893. doi:10.1016/j.msea.2021.140893

Xu, M., Yang, Y., Lei, H., Wang, P., Li, X., Zhang, Z., et al. (2020). Dynamic Response of Fiber Metal Laminates Subjected to Localized High Impulse Blast Loading. *Compos. Structures* 243 (December 2019), 112216. doi:10.1016/j.compstruct.2020.112216

Yao, L., Sun, G., He, W., Meng, X., and Xie, D. (2019). Investigation on Impact Behavior of FMLs under Multiple Impacts with the Same Total Energy: Experimental Characterization and Numerical Simulation. *Compos. Structures* 226 (June), 111218. doi:10.1016/j.compstruct.2019.111218

Zhan, J., Yao, X., Han, F., and Zhang, X. (2021). A Rate-dependent Peridynamic Model for Predicting the Dynamic Response of Particle Reinforced Metal Matrix Composites. *Compos. Structures* 263 (November 2020), 113673. doi:10.1016/j.compstruct.2021.113673

Zhang, K. F., Liang, M. Z., Li, X. Y., and Lu, F. Y. (2020). A Study on Fracture of Metal Plate under the Detonation Wave Interaction. *Int. J. Impact Eng.* 145 (July), 103665. doi:10.1016/j.ijimpeng.2020.103665

Zhang, S., Caprani, C. C., and Heidarpour, A. (2018). Strain Rate Studies of Pultruded Glass Fibre Reinforced Polymer Material Properties: A Literature Review. *Construction Building Mater.* 171, 984–1004. doi:10.1016/j.conbuildmat.2018.03.113

Zhao, N., Yao, S., Zhang, D., Lu, F., and Sun, C. (2020). Experimental and Numerical Studies on the Dynamic Response of Stiffened Plates under Confined Blast Loads. *Thin-Walled Structures* 154 (May), 106839. doi:10.1016/j.tws.2020.106839

Zhou, X., and Jing, L. (2020). Deflection Analysis of Clamped Square Sandwich Panels with Layered-Gradient Foam Cores under Blast Loading. *Thin-Walled Structures* 157 (August), 107141. doi:10.1016/j.tws.2020.107141

Conflict of Interest: The authors declare that the research was conducted in the absence of any commercial or financial relationships that could be construed as a potential conflict of interest.